Projected changes in the near-surface atmosphere over the Barents Sea based on CMIP5 scenarios

P. Verezemskaya[1], Yu. Selivanova[1], N. Tilinina[1], M. Markina[1], M. Krinitskiy[1], V. Sharmar[1], and O. Razorenova[1]

Received 15 September 2020; accepted 1 February 2021; published 28 May 2022.

Atmospheric climatological characteristics of the Barents Sea were analyzed in the model output of AMIP5 models for the present climate and climate projections under RCP4.5 and RCP8.5 scenarios for different periods of the 21st century. The results reveal strong changes in the mean surface air temperature amounting to more than 2 degrees during the 21st century. In line with this the frequency and duration of heat waves is increasing with the number and duration of the cold waves decreasing in course of the time period analyzed. Mean wind speed demonstrates upward changes under both RCP4.5 and RCP8.5 scenarios and these changes are accompanied by the upward change in the extreme wind speed over the Barents Sea at least for the first half of the century. The results are discussed in the context of potential changes in the atmospheric moisture transports which might be intensified during 21st century. *KEYWORDS:* Barents Sea; climate change; CMIP5 projections; surface temperature growth; marine ecology.

Citation: Verezemskaya, P., Yu. Selivanova, N. Tilinina, M. Markina, M. Krinitskiy, V. Sharmar, and O. Razorenova (2022), Projected changes in the near-surface atmosphere over the Barents Sea based on CMIP5 scenarios, *Russ. J. Earth. Sci., 22,* ES3003, doi:10.2205/2021ES000770.

1. Introduction

The largest air temperature growth over the globe of 3°C [*Zhang,* 2005] observed in the Arctic is regionally inhomogeneous [*Overland et al.,* 2011]. A positive trend in precipitation is observed in the Arctic [*Kattsov and Walsh,* 2000; *Pavelsky and Smith,* 2006]. Another important change is the ice-cover decline: during the satellite era summer sea-ice area was reduced by 50% [*Vihma,* 2014; *Onarheim et al.,* 2018], being 2.6 times faster than the yearly mean [*Shalina et al.,* 2018]. Since 1979 the sea ice-covered area in the Arctic is shrinking with the mean rate of 3% per year.

Enlarged open water area causes an increase of near-surface air temperature, thus eliminating meridional temperature gradient and zonal wind speed and contributing to the so-called "warm Arctic–cold Eurasia" pattern [*Petoukhov et al.,* 2013; *Wegmann et al.,* 2018]. This pattern is associated with the prolonged cold episodes over Eurasia in response to the warming over the Barents–Kara Sea (BKS) region. Another effect of sea-ice reduction is associated with surface albedo which is very different for seawater and ice [*Vihma et al.,* 2014; *Serreze et al.,* 2007 among others). Atmospheric response to sea-ice variability may also affect the stratosphere, particularly resulting in weakening of the polar vortex [*Cohen,* 2014; *Overland et al.,* 2016; *Yang,* 2016a].

Another effect is associated with wind waves and their impact on the upper ocean layer [*Young and Babanin,* 2006]. Under climate change characteristics of heat and gas exchange between the atmosphere and the ocean may change due to increased evaporation forced by wave breaking [*Andreas,* 2008; *Myslenkov et al.,* 2018; *Veron et al.,* 2008, 2011]. Notably wave-associated processes also affect the production of marine aerosol [*de Leeuw,* 2011] and impact on the ocean surface

[1]Shirshov Institute of Oceanology RAS, Moscow, Russia

http://rjes.wdcb.ru/doi/2021ES000770-res.html

Table 1. The Spatial Resolution of the Ocean and Atmospheric Components of Climate Models in Degrees Along the Longitude × Latitude.

MPI-ESM-MR		HadGEM2-ES		CCSM4	
ocean	atmosphere	ocean	atmosphere	ocean	atmosphere
$0.45 \times 0.45°$	$1.875 \times 1.875°$	$1 \times 0.83°$	$1.875 \times 1.25°$	$0.9375 \times 0.5625°$	$1.25 \times 0.9375°$

albedo [*Frouin et al.,* 2001]. All these factors may seriously change atmospheric moisture transports and associated weather conditions over European continent.

Various specific processes observed in the warming Arctic need to be correctly extrapolated under changing climate conditions. For example, the predominance of southern (northern) winds in winter (summer) claimed by *Kislov and Matveeva* [2020] to be driven by the monsoon-like circulation is expected to change in the 21st century with the land-sea temperature gradient. Current and projected opening of the sea surfaces and warming in winter may lead to increase or decrease of number of polar low occurrence [*Zahn and von Storch,* 2010; *Landgren et al.,* 2019].

In this study, we focus on the changes in the atmospheric conditions diagnosed for the present climate and projected by CMIP5 ensemble under two different climate scenarios (RCP4.5 and RCP8.5) in the experiments of Climate Models Intercomparison Project 5 [CMIP5, *Taylor et al.,* 2012]. The detailed regional assessment of the Barents Sea climate system has never been performed before and is crucial for understanding and analysis of the future changes in this region and associated changes in the moisture transports.

2. Data

We used data from the three numerical climate models from CMIP5 ensemble, specifically MPI-ESM-MR [*Giorgetta et al.,* 2013], HadGEM2-ES [*Collins et al.,* 2011] and CCSM4 [*Gent et al.,* 2011]. The MPI-ESM-MR model was developed at the Max Planck Institute (Hamburg, Germany) and combines the atmospheric model ECHAM6 [*Stevens et al.,* 2013], the ocean/ice model MPI-OM, the Earth surface model JSBACH, DYNVEG terrestrial biosphere model and HAMOCC ocean biogeochemistry model. Spatial resolution of the model varies from 10 km in the Arctic to 170 km in tropics (Table 1). The atmospheric model ECHAM6-MR is a hydrostatic spectral model with a spatial resolution of T63L95 Figure 1a. The HadGEM2-ES model is developed at the United Kingdom Metoffice and includes combined atmospheric and ocean modules from the Met Office Unified Model, the TRIFFID terrestrial vegetation, the diat-HadOCC ocean biogeochemistry model, and the UKCA atmospheric chemistry model. In the CCSM4 v.3 climate model developed by the US National Center for Atmospheric Research (Boulder, Colorado, USA) the ocean module is based upon the Parallel Ocean Program (POP). The model also includes Earth surface and vegetation from CLM and CICE ice model.

The spatial resolution of the ocean and atmosphere components of the analyzed models is shown in Table 1.

To analyze and predict climate changes in the Barents Sea, we analyzed historical period from 1979 to 2005, periods 2050–2059 and 2090–2099 for RCP4.5 scenario and periods 2030–2039, 2050–2059, and 2090–2099 for RCP8.5 scenario.

2.1. Methods

Maximum cold and warm atmospheric wave durations were calculated at each grid point for winter and summer periods as the number of days when extreme surface air temperature exceeded 10th and 90th percentile respectively at least for 5 days. Ice coverage period was assessed as the number of days in a year when ice concentration at a given point is higher than 15%. The ship icing risk parameter was calculated according to the Unified State System on the information of the World Ocean state criteria. The Barents Sea is characterized by fast icing type with icing rates of $(1.5 - 4.0) \times 10^3$ kg/hour, which is observed under the following conditions: wind

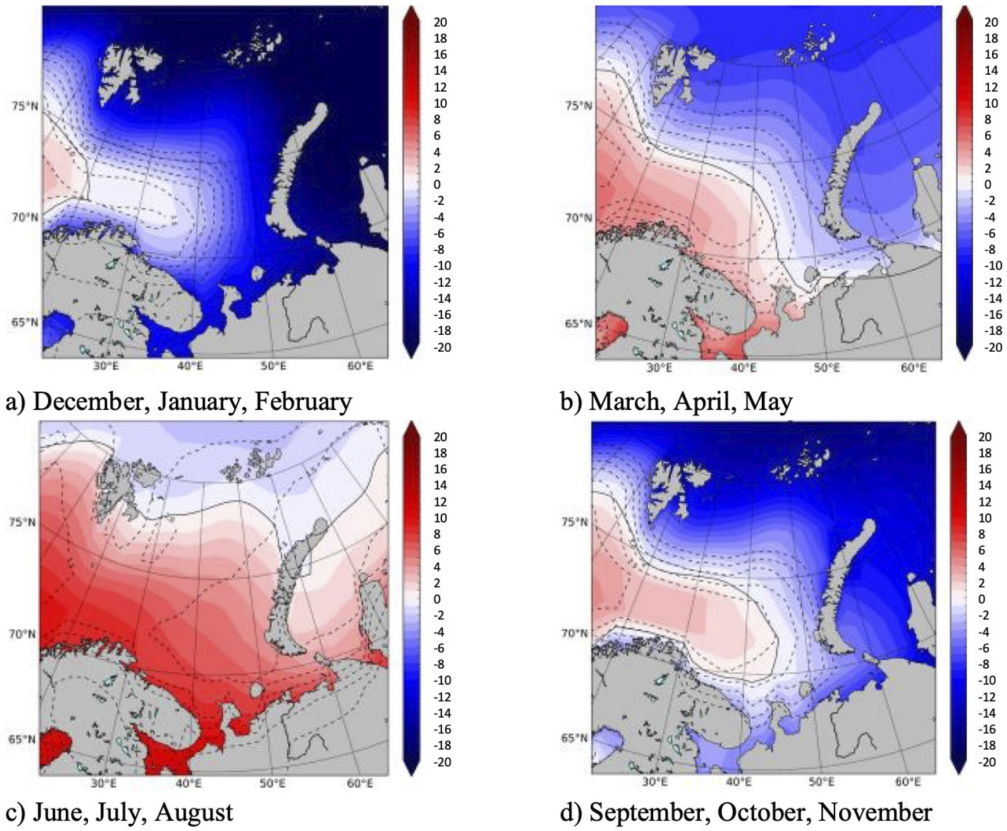

Figure 1. Mean air temperature at 2 m (°C) for the period 1979–2005 for different seasons: a) winter, b) spring, c) summer, d) autumn. Dashed line depicts the temperature standard deviation (°C) for the averaging period.

speed exceeding 10 m/s, air temperature lower than −4°C and fog or precipitation. Normally fog is determined as 100% relative humidity, but in the polar regions it may be observed with lower saturation, thus we choose 95% as a threshold. In case when all conditions were satisfied the day was marked by a flag. The number of days in each year then was averaged overall period. Extreme wind speeds were estimated as 95th, 99th, and 99.9th percentiles of scalar wind speed distribution. The coastlines of the Barents Sea were set according to the Navigation and Oceanography Department of the Russian Ministry of Defense and adjusted for model spatial resolution.

3. Results: Modern Climate

During historical period, near-surface air temperature over the Barents Sea (hereinafter – BS) has increased by +3.5°C. This increase is caused by the global temperature signal and the local factors associated with the melting sea ice. Between 1979 and 2005 the ice area in the BS decreased at the pace -10.6×10^3 km^2 (10.7% of the total area) per year [*Yang et al.*, 2016b].

Mean air temperature over all models for the period 1979–2005 over the Barents Sea was found to be −1.25°C. During winter season in the north-eastern part of the sea the air temperature drops to −20... − 25°C with the −20° isotherm following the position of the ice cover margin in January–February. Such low values are caused by the impact of dry air above the ice surface in the absence of solar radiation input. In the western part of the sea, the average winter air temperature is 2°C (Figure 1a).

The average temperature in spring (−1.2°) is higher than that in the autumn (−4.3°), that is caused by the warming effect of the land. In the spring and autumn seasons in the western part of the sea the air temperature is ranging between +3... + 4°C, while in the southern part in spring,

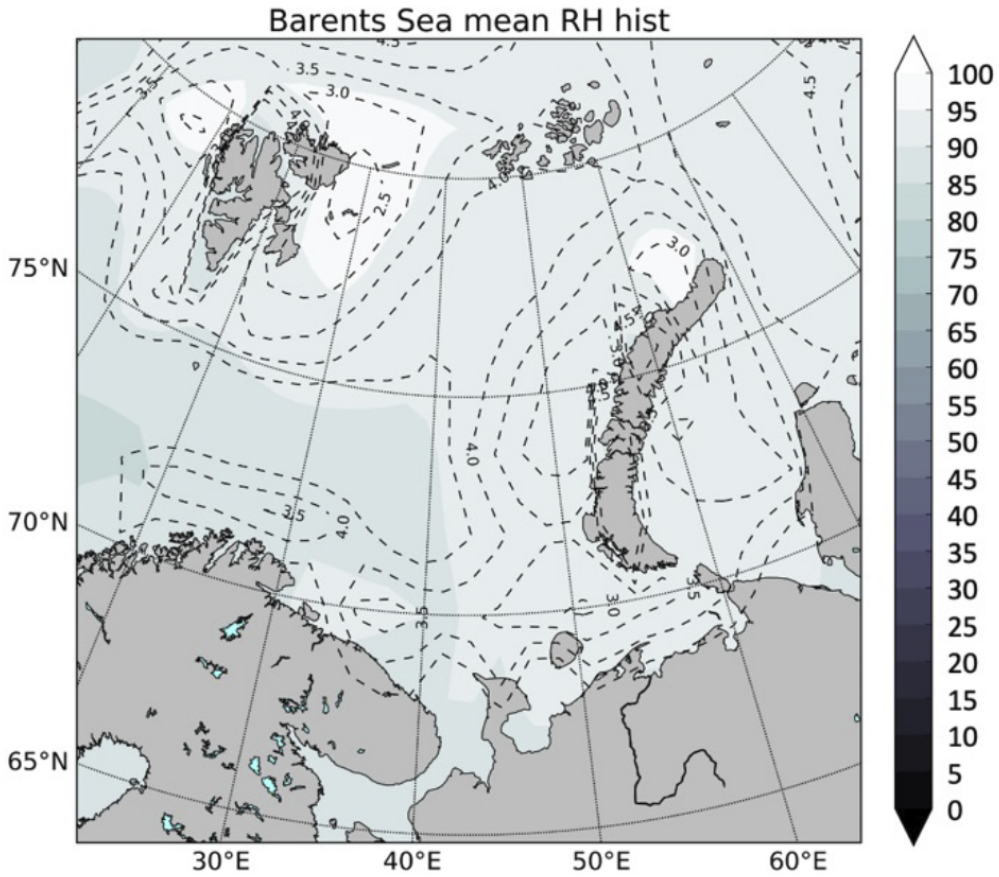

Figure 2. Mean relative humidity of the air at 2 m (%) for the period 1979–2005. Dashed line depicts the standard deviation of RH for the averaging period.

the average air temperature amounts to +6... + 7° (Figure 1b, Figure 1d). The average maximum air temperature in the region is observed in August and varies from +20°C over the Kanin Peninsula to 0°C north of Spitsbergen and Novaya Zemlya. In general, islands and archipelagos have a cooling effect on the area-averaged temperatures.

The average annual relative humidity (RH) over the BS ranges from 75 to 100% (Figure 2) and varies slightly from season to season (no more than 5% of the absolute value). During autumn and winter RH field is determined by the position of the warm current (high values) and island archipelagos (low values). In summer and spring RH shows south-north pattern with high values in the south, and low values in the north.

High probability of air saturation and condensation, as well as the frequent temperature inversions (surface temperature is lower than at 1.5–2 km), during the air advection episodes in the warm sectors of cyclones, provides the conditions for the formation of low-level strato-cumulus clouds. The highest average cloud cover is observed in the summer season being close to overcast (95–100%) over most of BS. The smallest cloud cover of 75% is observed during spring.

Wind regime of the Barents Sea (Figure 3) is largely determined by the frequent storms associated with extra-tropical and mesoscale cyclones, as well as with local phenomena such as Novaya Zemlya Bora. In winter the region is dominated by mean winds of the south and north-east direction (Figure 3a) with speeds of 2–4 m/s what agrees well with latest results of *Kislov and Matveeva* [2020]. From autumn to spring the direction varies from north-north-east to south-east, with the average maximum wind speed increasing from 2 m/s to 4 m/s in the north-western part of the sea (Figure 4b, Figure 4c, Figure 4d). Different estimates report from 11 to 14 intense polar mesocyclones

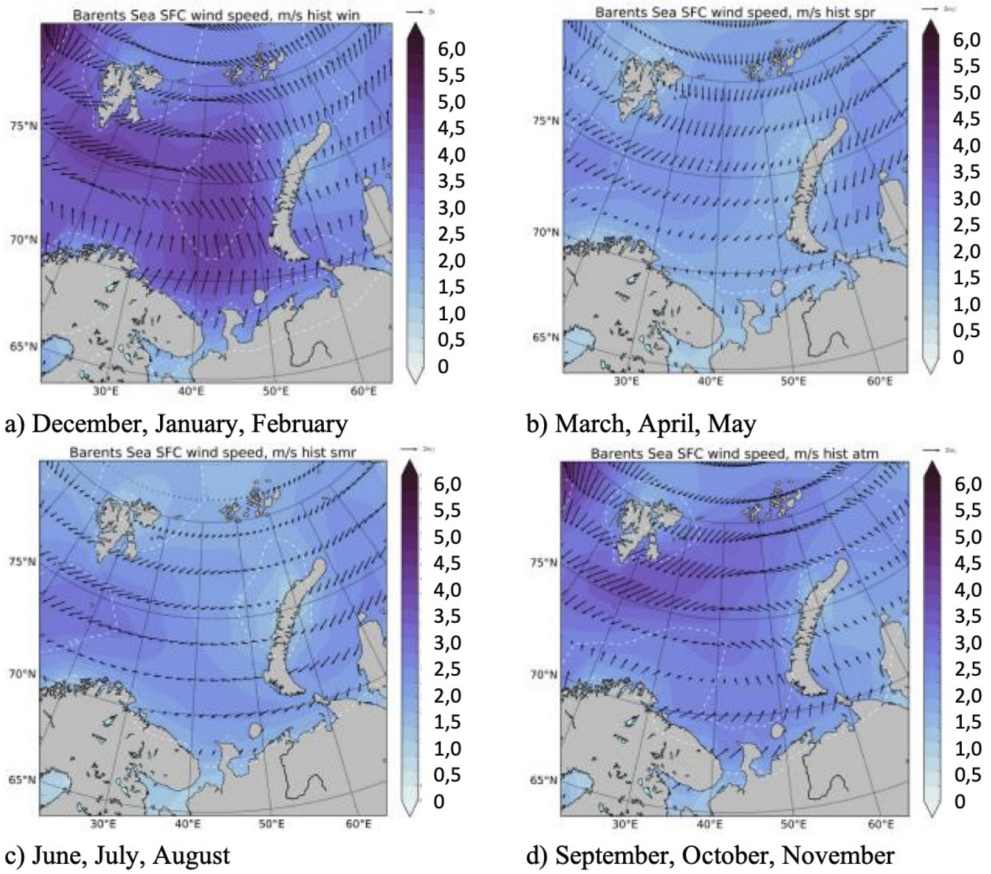

Figure 3. Mean surface wind speed (m/s, in color) and direction (black arrows) at 10 meters for 1979–2005 seasons: a) winter, b) spring, c) summer, d) autumn. Dashed line depicts the wind speed standard deviation (m/s) for the averaging period.

per year over the BS [*Noer et al.,* 2011; *Rojo et al.,* 2015; *Smirnova et al.,* 2016]. Polar mesocyclones are characterized by wind speeds exceeding gale force (15 m/s) and are usually associated with high values of heat fluxes (> 1000 W/m^2), significantly affecting the characteristics of the ocean mixed layer [*Condron et al.,* 2008; *Gulev and Belyaev,* 2012; *Tilinina et al.,* 2018].

4. Climate Projections

To describe the future climate in the Barents Sea, we analyzed from the model output air temperature at 2 meters, cloud cover, number of days with a probability of fog formation, precipitation, wind direction and speed and the number of days with a probability of icing of ships. In the following all the estimates of the changes are given relative to the base period 1979–2005.

Air temperature has quickly increased relative to the base period in both medium and extreme warming scenarios. The average winter season temperature for the entire BS increases from -6.1°C and -5.66° to -1.8°C and $+1.7$°C in RCP4.5 and RCP8.5 respectively during 2030–2039. Summer temperatures rise from 6.6°and 7.4°C to 10.3°C and 13.1°C in RCP4.5 and RCP8.5 during the same period. Figure 4 shows air temperature probability distributions for different seasons for the periods 2030–2039 and 2090–2099 for the two scenarios. The shape of probability distributions changes over the century, especially in the winter and summer seasons. Compared to 2030–2039 in the period 2090–2099 winter occurrence of extremely low temperatures (-15° to -25°C) decreases significantly from 30% to 5%. We have to note that a more aggressive scenario RCP8.5 is characterized by the lower temperature compared to RCP4.5 implying a more stable state of the temperature regime.

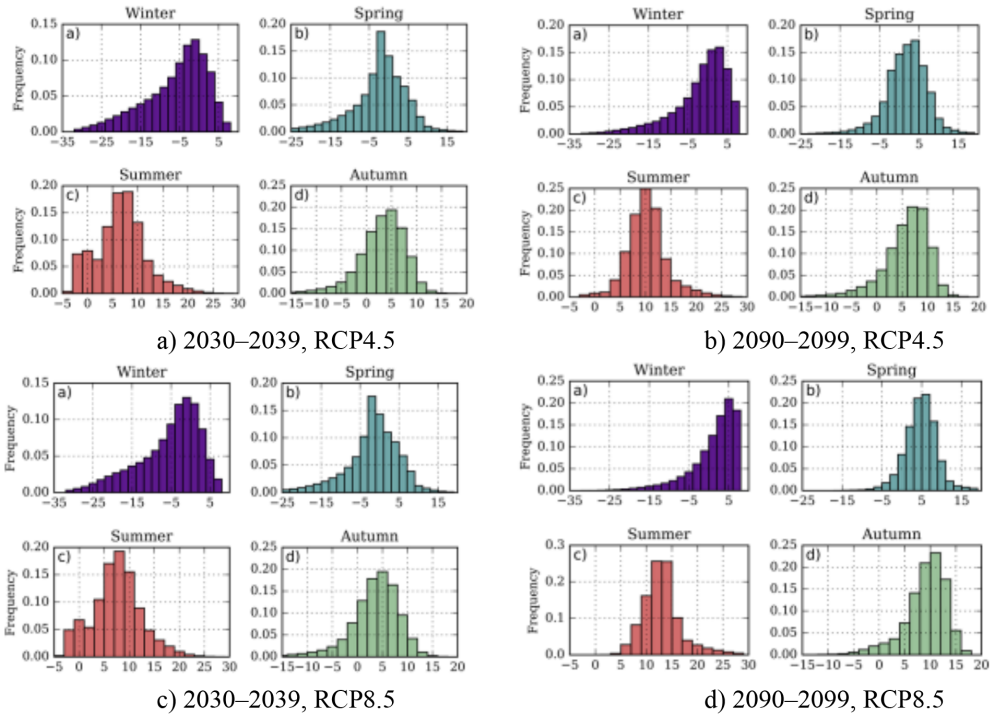

Figure 4. Probability distribution function of daily mean air temperature (°C) according to the a) short-term and b) long-term mild warming scenario and c) short-term and d) long-term extreme warming scenario.

Changing the shape of the summer temperature distribution hints on the change in the temperature regime over the BS. Bimodal distribution at the beginning of the century reflecting the presence of the Arctic and midlatitudinal air masses during summer tends to evolve to the close to Gaussian distribution, implying the shift towards the midlatitudinal temperature conditions.

Change in the temperature regime of the BS is also evident in the increase in the extreme temperature values. According to the RCP8.5 scenario, the annual mean and monthly temperature increases from 3.5°to 7.5°C, while the mean minimum temperature increases by 10°C, from −10° to 0°C.

Changes in the temperature regime over the Barents Sea result in the increase of the probability of heat and cold waves. RCP4.5 scenario projects a decrease in the number of cold waves over the Barents Sea in summer from 4.5 to 1.5–4 events per season between 2030–2039 and 2090–2099. The average duration of cold waves in summer changes from 6–9 days to up to 10 days under RCP4.5 scenario. In summer the number of heat waves lasting at least 5 days increases during the century from 2.7 to 3.2 events. The maximum increase in the number of heat waves is projected in the central and the northeastern parts of the sea.

In winter the number of cold waves decreases from $\sim$ 3 events per season in the present conditions to 2.6 waves per season during 2030–2039. During the period 2030–2039 areas most affected by cold waves are identified in the southern part of the sea, while in the middle of the century cold events may occupy the entire sea domain and increase in frequency. The average maximum duration of the cold waves in the winter changes from $\sim$ 7 days during 2030–2039 to 5.8 days at the end of the century.

The wind speed characteristics were significantly changed in line with the change in the thermal regime during the 21st century. Under RCP4.5 scenario in summer the mean wind speed ranges within 2–3.25 m/s (Figure 5), however, the maximum wind region shifts from the western part to the northeast compared to the present climate conditions. Between 2030–2039 and 2090–2099 dominating wind direction changes from the east-southeastern to northeastern. During the same

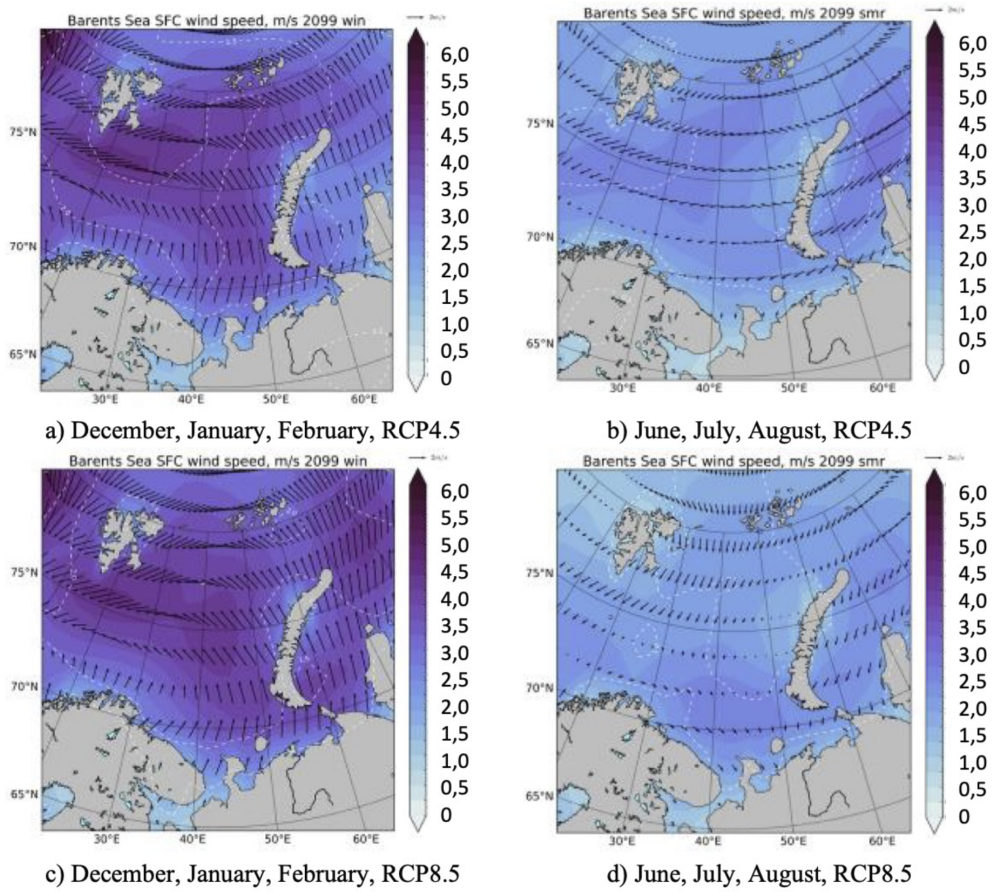

Figure 5. Mean wind speed (m/s, color) and direction (arrows) at 10 meters during 2090–2099 in (a) winter and (b) summer according to RCP4.5 scenario and (c), (d) RCP8.5. Dashed line depicts the standard deviation of wind speed (m/s) over the averaging period.

time winter mean wind speed decreases from 6 m/s to 4.5 m/s, reaching its minimum in the middle of the century (2050–2059). The local maxima observed south of Svalbard and north of Kolguev isle, almost disappear in the middle of the century, with winds being 4–5 m/s in 2090–2099 (Figure 5a, Figure 5b). Under RCP8.5 scenario summer wind speed decreases over the century and changes its dominant direction from the northeastern to the northern (Figure 5c, Figure 5d). The mean wintertime wind speed shows an increase form 4 m/s to 6–7 m/s during the century.

Different climate warming scenarios project also different changes in extreme wind characteristics. These changes are qualitatively the same for different percentiles. Thus, under RCP4.5 scenario the maximum wind speed quantified as 99.9th percentile changes from 24 m/s for 2030–2039 to 27 m/s during 2050–2059, while then experiences downward tendency until the end of the century (Figure 6). Notably under RCP8.5 scenario the tendency between the periods 2050–2059 and 2090–2099 is opposite and implies continuously growing wind speed (Figure 6).

5. Conclusions and Discussion

We provided the first comprehensive assessment of the regional changes in climatological characteristics of the Barents Sea as revealed by CMIP5 models from the present climate condition (1979–2005) onwards for the moderate and aggressive warming scenarios RCP4.5 and RCP8.5. We conclude that the mean winter air temperature over the entire Barents Sea increases from $-6.1°C$ and $-5.66°C$ in RCP4.5 and RCP8.5 scenarios respec-

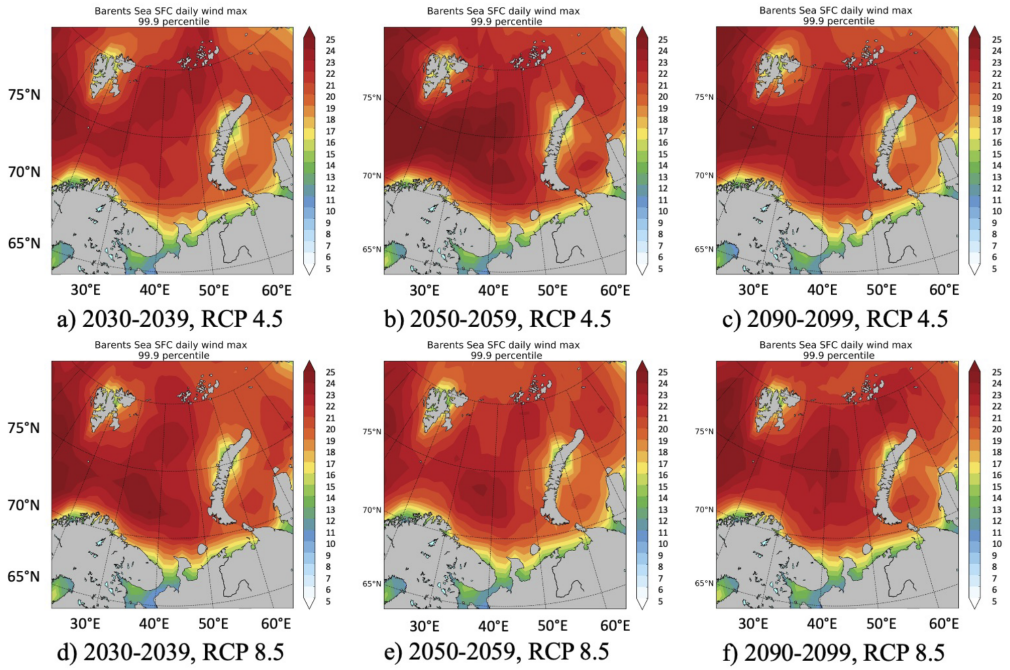

Figure 6. 99.9th percentile wind speed at 10 meters in the Barents Sea according to (a, b, c) RCP4.5 scenario and (d, e, f) RCP8.5 scenario for periods (a, d) 2030–2039, (b, e) 2050–2059 and (c, f) 2090–2099.

tively to −1.8°C and +1.7°C in the same scenarios between 2030–2039 and the end of the century. Summer temperatures are also rising from 6.6°C and 7.4°C (in RCP4.5 and RCP8.5) to 10.3°C and 13.1°C. We discovered that bimodal probability distribution of air temperature over the Barents Sea in the beginning of the century experiences the transition to the Gaussian-like distribution with a shift of the mean towards higher temperature values. Under RCP4.5 scenario the number of cold waves over the Barents Sea increases from 2.6 to 3.7 events per season between 2030–2039 and 2090–2099. The number of heatwaves in summer is increasing over the century from 2.7 to 3.2 events per season. Simultaneously the number and the duration of cold waves over the Barents Sea decreases in winter, while there is an increase in the number of cold waves in summer. We demonstrated changes in the structure of wind speed pattern throughout the century and the decrease of the mean wind speed during winter from 6 m/s to 4.5 m/s from the beginning of 21st century to the period 1950–1959. This is consistent with changes in the magnitude of extreme winds in the first part of century under both RCP4.5 and RCP8.5 scenarios.

The results of the paper can be first of all discussed in the content of the role of Barents Sea in the moisture transport in the present and future climate. Ocean climate signals are translated into the changes in atmospheric moisture transports as the ocean evaporation provides the major source of the atmospheric moisture. In this respect the role of the Barents Sea in the moisture advection to European Russia can seriously change in course of the 21st century. Declining sea ice extent and changes in temperature and winds may impose preconditioning for the abrupt growth of local evaporation. On the other hand, "warm Arctic–cold Eurasia" pattern can work in a way providing conditions for ocean to land moisture transports. In the present climate atmospheric moisture transports in this region are primarily directed to the north providing moisture injections to the Arctic [*Dufour et al.*, 2016] with considerable fraction of the transported moisture being advected in the cyclones which also experience changes in the Arctic [*Tilinina et al.*, 2014]. However, with climate change situations favorable for the ocean-to-land moisture advection might become more frequent. Figure 7 shows two recent examples of the

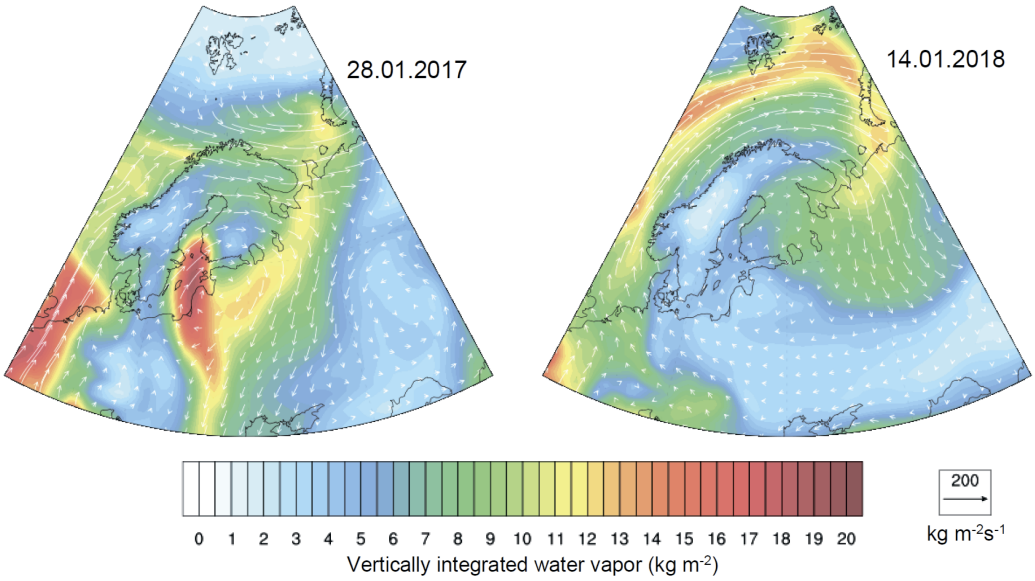

Figure 7. Two examples of the distribution of the vertically integrated water vapor content and water vapor transport for 28.01.2017 (left) and 14.01.2018 (right).

distribution of the vertically integrated water vapor content and water vapor transport diagnosed from the ERA-Interim. These examples clearly demonstrate that even in the present climate situations associated with the strong moisture transports from the Arctic Ocean to European Russia can occur and provide increases in the moisture content over northern European Russia and the whole Eastern Europe. Associated anomalies of the vertically integrated atmospheric moisture content may amount to 20 kg/m^2 being and order of magnitude stronger compared to the background values. In this respect further analysis of the local atmospheric moisture advection and its association with the climate signals over the Barents Sea on the basis of CMIP5 model output are highly desirable. Importantly, climate models have typically relatively coarse resolution that might limit capabilities of the accurate diagnostics of moisture transports. In this respect high resolution experiments with non-hydrostatic models [e.g. *Gavrikov et al.*, 2020] would be extremely useful for downscaling climate model results. This might help to also accurately analyze the role of mesoscale phenomena, such as Novaya Zemlya Bora in forming local moisture conditions.

Acknowledgments. This work was undertaken with financial support by the MEGA grant 14.W03.31.0006. Inter-annual variability analysis was conducted under RSCF grant No. 20-17-00139

References

Andreas, E. L., P. O. G. Persson, J. E. Hare (2008), A Bulk Turbulent Air-Sea Flux Algorithm for High-Wind, Spray Conditions, *Journal of Physical Oceanography*, *38,* No. 7, 1581–1596, **Crossref**

Cohen, J., J. A. Screen, et al. (2014), Recent Arctic amplification and extreme mid-latitude weather, *Nature Geoscience*, *7,* No. 9, 627–637, **Crossref**

Collins, W. J., N. Bellouin, et al. (2011), Development and evaluation of an Earth-System model – HadGEM2, *Geoscientific Model Development*, *4,* No. 4, 1051–1075, **Crossref**

Condron, A., G. R. Bigg, I. A. Renfrew (2008), Modeling the impact of polar mesocyclones on ocean circulation, *Journal of Geophysical Research: Oceans*, *113,* No. 10, **Crossref**

Dufour, A., O. Zolina, S. K. Gulev (2016), Atmospheric moisture transport to the Arctic: Assessment of reanalyses and analysis of transport components, *Journal of Climate*, *29,* No. 14, 5061–5081, **Crossref**

Frouin, R., S. F. Iacobellis, P. Y. Deschamps (2001), Influence of oceanic whitecaps on the Global Radiation Budget, *Geophys. Res. Lett.*, *28,* No. 8, 1523–1526, **Crossref**

Gavrikov, A., S. K. Gulev, et al. (2020), RASNAAD: 40-yr High-Resolution North Atlantic atmo-

spheric hindcast for multipurpose applications (new dataset for the regional mesoscale studies in the atmosphere and the ocean), *Journal of Applied Meteorology and Climatology*, *59,* No. 5, 793–817, **Crossref**

Gent, P. R., et al. (2011), The Community Climate System Model Version 4, *Journal of Climate*, *24,* No. 19, 4973–4991, **Crossref**

Giorgetta, M. A., J. Jungclaus, et al. (2013), Climate and carbon cycle changes from 1850 to 2100 in MPI-ESM simulations for the Coupled Model Intercomparison Project phase 5, *Journal of Advances in Modeling Earth Systems*, *5,* No. 3, 572–597, **Crossref**

Gulev, S. K., K. Belyaev (2012), Probability distribution characteristics for surface air–sea turbulent heat fluxes over the global ocean, *Journal of Climate*, *25,* No. 1, 184–206, **Crossref**

Kattsov, V. M., J. E. Walsh (2000), Twentieth-century trends of Arctic precipitation from observational data and a climate model simulation, *Journal of Climate*, *13,* No. 8, 1362–1370, **Crossref**

Kislov, A., T. Matveeva (2020), The Monsoon over the Barents Sea and Kara Sea, *Atmospheric and Climate Sciences*, *10,* 339–356, **Crossref**

Landgren, O. A., Y. Batrak, et al. (2019), Polar low variability and future projections for the Nordic and Barents Seas, *Q. J. R. Meteorol. Soc.*, *145,* 3116–3128, **Crossref**

De Leeuw, G., E. L. Andreas, et al. (2011), Production flux of sea spray aerosol, *Reviews of Geophysics*, *49,* No. 2, **Crossref**

Myslenkov, S., A. Medvedeva, et al. (2018), Long-term statistics of storms in the Baltic, Barents and White seas and their future climate projections, *Geography, Environment, Sustainability*, *11,* No. 1, 93–112, **Crossref**

Noer, G., et al. (2011), A climatological study of polar lows in the Nordic Seas, *Q. J. R. Meteorol. Soc.*, *137,* No. 660, 1762–1772, **Crossref**

Onarheim, I. H., T. Eldevik, et al. (2018), Seasonal and regional manifestation of Arctic sea ice loss, *Journal of Climate*, *31,* No. 12, 4917–4932, **Crossref**

Overland, J. E., M. Wang (2016), Recent extreme Arctic temperatures are due to a split polar vortex, *Journal of Climate*, *29,* No. 15, 5609–5616, **Crossref**

Overland, J. E., K. R. Wood, M. Wang (2011), Warm Arctic – cold continents: climate impacts of the newly open Arctic Sea, *Polar Research*, *30,* No. 1, 15,787, **Crossref**

Pavelsky, T. M., L. C. Smith (2006), Intercomparison of four global precipitation data sets and their correlation with increased Eurasian river discharge to the Arctic Ocean, *Journal of Geophysical Research: Atmospheres*, *111,* No. D21, **Crossref**

Petoukhov, V., S. Rahmstorf, et al. (2013), Quasiresonant amplification of planetary waves and recent Northern Hemisphere weather extremes, *Proceedings of the National Academy of Sciences*, *110,* No. 14, 5336–5341, **Crossref**

Rojo, M., C. Claud, et al. (2015), Polar low tracks over the Nordic Seas: A 14-winter climatic analysis, *Tellus A: Dynamic Meteorology and Oceanography*, *67,* No. 1, 24,660, **Crossref**

Serreze, M. C., M. M. Holland, J. Stroeve (2007), Perspectives on the Arctic's shrinking sea-ice cover, *Science*, *315,* No. 5818, 1533–1536, **Crossref**

Shalina, E. V., S. Sandven (2018), Snow depth on Arctic Sea ice from historical in situ data, *The Cryosphere*, *12,* No. 6, 1867–1886, **Crossref**

Smirnova, J. E., E. V. Zabolotskikh, et al. (2016), Statistical characteristics of polar lows over the Nordic Seas based on satellite passive microwave data, *Izv. Atmos. Ocean. Phys.*, *52,* No. 9, 1128–1136, **Crossref**

Stevens, B., et al. (2013), Atmospheric component of the MPI-M Earth System Model: ECHAM6, *J. Adv. Model. Earth Syst.*, *5,* 146–172, **Crossref**

Taylor, K. E., R. J. Stouffer, G. A. Meehl (2012), An overview of CMIP5 and the experiment design, *Bulletin of the American meteorological Society*, *93,* No. 4, 485–498, **Crossref**

Tilinina, N., A. Gavrikov, S. K. Gulev (2018), Association of the North Atlantic surface turbulent heat fluxes with midlatitude cyclones, *Monthly Weather Review*, *146,* No. 11, 3691–3715, **Crossref**

Tilinina, N., S. K. Gulev, D. H. Bromwich (2014), New view of Arctic cyclone activity from the Arctic system reanalysis, *Geophysical Research Letters*, *41,* No. 5, 1766–1772, **Crossref**

Veron, F., W. K. Melville, L. Lenain (2008), Wave-Coherent Air–Sea Heat Flux, *J. Phys. Oceanogr.*, *38,* No. 4, 788–802, **Crossref**

Veron, F., W. K. Melville, L. Lenain (2011), The effects of small-scale turbulence on air–sea heat flux, *Journal of Physical Oceanography*, *41,* No. 1, 205–220, **Crossref**

Vihma, T. (2014), Effects of Arctic Sea ice decline on weather and climate: A review, *Surveys in Geophysics*, *35,* No. 5, 1175–1214, **Crossref**

Vihma, T., R. Pirazzini, et al. (2014), Advances in understanding and parameterization of small-scale physical processes in the marine Arctic climate system: a review, *Atmospheric Chemistry and Physics*, *14,* No. 17, 9403–9450, **Crossref**

Wegmann, M., Y. Orsolini, O. Zolina (2018), Warm Arctic – cold Siberia: comparing the recent and the early 20th-century Arctic warmings, *Environmental Research Letters*, *13,* No. 2, 025009, **Crossref**

Yang, H., G. Lohmann, et al. (2016a), Intensification and poleward shift of subtropical western boundary currents in a warming climate, *Journal of Geophysical Research: Oceans*, *121,* No. 7, 4928–4945, **Crossref**

Yang, X. Y., X. Yuan, M. Ting (2016b), Dynamical link between the Barents–Kara sea ice and the Arctic Oscillation, *Journal of Climate*, *29,* No. 14, 5103–5122, **Crossref**

Young, I. R., A. V. Babanin (2006), Spectral distribution of energy dissipation of wind-generated waves due to dominant wave breaking, *Journal of Physical Oceanography*, *36,* No. 3, 376–394, **Crossref**

Zahn, M., H. von Storch (2010), Decreased frequency of North Atlantic polar lows associated with future climate warming, *Nature*, *467,* No. 7313, 309–312, **Crossref**

Zhang, J. (2005), Warming of the arctic ice–ocean system is faster than the global average since the 1960s, *Geophysical Research Letters*, *32,* No. 19, **Crossref**

Corresponding author:
Polina Verezemskaya, Shirshov Institute of Oceanology RAS, 36 Nahimovskiy Pr., 117997 Moscow, Russia. (verezem@sail.msk.ru)